International Journal of Environmental Sciences
ISSN: 2229-7359
Vol. 11 No. 22s, 2025
https://theaspd.com/index.php

Synthesis, Characterization: Novel Nano Copolymer-Amoxicillin Drug Composite as a Potential Treatment of Breast Cancer Cell Line (MCF-7): Molecular Docking and Biological Activity

Hussein H. M. Al-Masoudi[1], Karim Akbari Dilmaghani[1], Mohammad N. AL-Baiati[2]
[1]Faculty of Science, Department of Chemistry, Urmia University, Urmia, Iran
[2]University of Kerbala, College of Education for Pure Sciences, Department of Chemistry, Karbala, Iraq

Abstract: *In this study, a novel nano copolymer–amoxicillin drug composite was synthesized and evaluated for its potential anticancer activity against the MCF-7 breast cancer cell line. The nano copolymer was prepared through a polycondensation reaction involving glycerol (2 mol) and phthalic anhydride (4 mol), and its structure was confirmed using FT-IR, ^{1}H NMR, ^{13}C NMR, X-ray diffraction (XRD), transmission electron microscopy (TEM), and atomic force microscopy (AFM). The functionalization of the copolymer with amoxicillin (1 mol) yielded a nano drug composite, which was similarly characterized by spectroscopic methods. Molecular docking analysis was conducted to investigate the interaction between the drug composite and key breast cancer-related proteins, revealing favorable binding interactions that suggest a potential mechanism of therapeutic action. In vitro cytotoxicity assays against MCF-7 cells demonstrated significant anticancer activity, with an IC_{50} value of 55.09 μg/mL. These findings highlight the potential of the synthesized nano drug composite as a promising candidate for targeted breast cancer therapy.*

Keywords: *Nano copolymer, Amoxicillin, Drug composite, Molecular docking, Breast cancer, MCF-7 cell line, Cytotoxicity.*

Corresponding author: (Hussein H. M. Al-Masoudi, Email: K.adilmaghani@urmia.ac.ir)

INTRODUCTION

Nanotechnology refers to the manipulation and application of materials at the nanoscale—typically one billionth of a meter (1×10^{-9} m). To offer perspective, a nanometer is approximately 100,000 times smaller than the width of a human hair. Common examples of nanomaterials include nanoparticles, nanotubes, and nanofibers, each of which offers unique physical, chemical, and biological properties. The advent of nanotechnology has led to transformative advances across multiple disciplines, particularly in medicine, where it plays a pivotal role in drug delivery, diagnostics, biosensing, and tissue engineering [1–4].

Breast cancer is the most frequently diagnosed cancer and a leading cause of cancer-related deaths among women worldwide, especially in developed nations such as the United States [5]. It arises from the uncontrolled proliferation of cells within breast tissue, which can form malignant tumors. Symptoms include palpable lumps, visible changes in breast shape or texture, and inverted nipples [6]. As the disease progresses, cancer cells may metastasize to nearby lymph nodes or distant organs, significantly complicating treatment [7,8].

One of the most promising approaches in modern oncology is nanocarrier-based drug delivery. These systems are designed to encapsulate therapeutic agents and deliver them precisely to the target site. Such platforms enhance drug bioavailability, reduce enzymatic degradation, and minimize off-target side effects. Upon reaching the targeted tissue, the nanocarrier facilitates cellular uptake and subsequently releases the drug at the intracellular site of action [9,10].

Amoxicillin is a β-lactam antibiotic belonging to the aminopenicillin subclass. It is widely used to treat various bacterial infections due to its broad-spectrum antimicrobial activity and excellent safety profile [11]. Interestingly, recent research has suggested that certain antibiotics, including amoxicillin, may exert additional biological effects such as modulating cellular pathways involved in tumor progression, making them candidates for drug repurposing in cancer therapy [12].

The present study aims to synthesize and characterize a novel nano copolymer system functionalized with amoxicillin. The copolymer was prepared via a polycondensation reaction using glycerol and phthalic anhydride, followed by the conjugation of amoxicillin to produce a targeted drug composite. Advanced characterization techniques, including FT-IR, NMR, XRD, TEM, and AFM, were employed to confirm

the structural and morphological features of the nanocomposite. Furthermore, molecular docking simulations were conducted to predict the drug's interaction with breast cancer-related proteins, and in vitro cytotoxicity assays were used to evaluate the anticancer potential of the composite against the MCF-7 breast cancer cell line [13].

This work contributes to the growing field of nano-enabled drug delivery systems and demonstrates the potential of antibiotic-functionalized nanomaterials for targeted cancer therapy.

METHODOLOGY

Synthesis of Nano Copolymer

Phthalic anhydride (5.0 mol, 740 g) was dissolved in 7.5 mL of dimethyl sulfoxide (DMSO) in a 125 mL beaker equipped with a thermometer. The mixture was heated to 155 °C and stirred continuously using a magnetic stirrer for 20 minutes, resulting in a colorless liquid. Subsequently, glycerol (2.0 mol, 184 g) was added to initiate the polycondensation reaction.

To facilitate the removal of water produced during esterification, approximately 10 mL portions of xylene were gradually introduced. After an additional 15 minutes of reaction, the heating was discontinued. The reaction mixture was then poured into cold deionized water (3 °C) to precipitate the product. The resulting solid was collected by filtration, washed thoroughly with deionized water, and dried at room temperature. Finally, the dried solid was pulverized to obtain the nano copolymer as illustrated in Equation 1 [3].

Synthesis of Acid Chloride of Nano Copolymer

To prepare the acid chloride derivative, 0.6 g of the previously synthesized nano copolymer was mixed with 4–5 drops of thionyl chloride ($SOCl_2$) and 6.0 mL of dichloromethane (DCM) in a 25 mL beaker. The mixture was stirred magnetically and allowed to rest at room temperature for 30 minutes to enable initial activation. It was then heated to 65 °C and maintained for 2 hours to promote acyl chloride formation. Finally, the temperature was increased to 85 °C and maintained for an additional 2 hours to ensure complete conversion. The resulting nano copolymer–acid chloride product was collected and used in the next step of the synthesis [14], as illustrated in Equation 2.

Synthesis of Nano Drug Composite

Amoxicillin (1.5 g, 1.0 mol) was dissolved in 8 mL of dichloromethane (DCM) along with 0.5 mL of triethylamine under continuous stirring in an ice bath. This solution was slowly added to the acid chloride-modified nano copolymer prepared in the previous step (0.6 g). The resulting mixture was transferred into a 50 mL beaker containing crushed ice and stirred thoroughly with a glass rod until the ice melted and a precipitate formed.

The solid product was filtered, washed, and then stirred in an ice bath for 1 hour, followed by additional stirring at room temperature for 3 hours to complete the reaction. The obtained drug-loaded nano composite was dried and characterized accordingly [15], as shown in Equation 3.

Molecular Docking

Molecular docking studies were conducted to evaluate the interaction between the synthesized nano drug composite and key protein targets involved in breast cancer. The docking simulations were carried out using PyRx and Biovia software integrated with the Molecular Operating Environment (MOE) module. These tools enabled the prediction of binding affinities, identification of key amino acid residues involved in drug–receptor interactions, and visualization of molecular conformations. The results provided insight into the potential binding mechanisms and biological relevance of the synthesized compound [16].

Biological Activity

MCF-7 human breast cancer cells were cultured in RPMI-1640 medium supplemented with 10% fetal bovine serum (FBS), 100 U/mL penicillin, and 100 µg/mL streptomycin. Cells were maintained under standard conditions in a humidified incubator at 37 °C with 5% CO_2. Cells were passaged using trypsin-EDTA and seeded at approximately 80% confluency for experiments [3,17].

Cytotoxicity Assay

The cytotoxic effect of the nano amoxicillin drug composite was evaluated using the MTT assay in 96-well plates. MCF-7 cells were seeded at a density of 1×10^4 cells per well and allowed to adhere for 24 hours.

The cells were then treated with varying concentrations of the nano drug composite and incubated for 72 hours.

After treatment, the culture medium was removed, and 100 µL of MTT solution (0.002 mg/mL) was added to each well. The cells were incubated at 37 °C for 2.5 hours to allow formazan crystal formation. Following incubation, the MTT solution was removed, and 130 µL of dimethyl sulfoxide (DMSO) was added to dissolve the formazan crystals. The plate was shaken gently and incubated at 37 °C for an additional 15 minutes. Absorbance was measured at 492 nm using a microplate reader.

Cell viability and inhibition rate were calculated using the following formula:

$$\text{Inhibition rate} = \frac{(A-B)}{A} \times 100$$

Where:

A = absorbance of control (untreated cells)

B = absorbance of treated sample

All experiments were conducted in triplicate.

Data Analysis

Statistical analysis was performed using the unpaired Student's t-test in GraphPad Prism (version 6). Results are presented as mean ± standard deviation (SD) based on three independent experimental replicates. A p-value < 0.05 was considered statistically significant [18].

RESULTS AND DISCUSSION

Synthesis and Characterization of the Nano Copolymer and Its Acid Chloride

The nano copolymer was successfully synthesized following the procedure outlined in the methodology section, involving the polycondensation of glycerol and phthalic anhydride. The resulting material was purified and characterized using various analytical techniques, including FT-IR, ^{1}H NMR, ^{13}C NMR, X-ray diffraction (XRD), transmission electron microscopy (TEM), and atomic force microscopy (AFM), to confirm its structure, morphology, and nanoscale features.

Spectroscopic analysis (FT-IR, NMR) confirmed the formation of ester linkages and the preservation of functional groups within the polymer backbone. The copolymer's transformation into its acid chloride derivative was further confirmed by the appearance of characteristic peaks in the FT-IR spectrum, indicating successful chlorination of the terminal carboxylic acid groups.

The synthetic steps are summarized in Equation (1) for the nano copolymer formation and Equation (2) for the preparation of the nano copolymer acid chloride. These foundational compounds were used in subsequent steps for the conjugation with amoxicillin to form the drug-loaded nanocomposite.

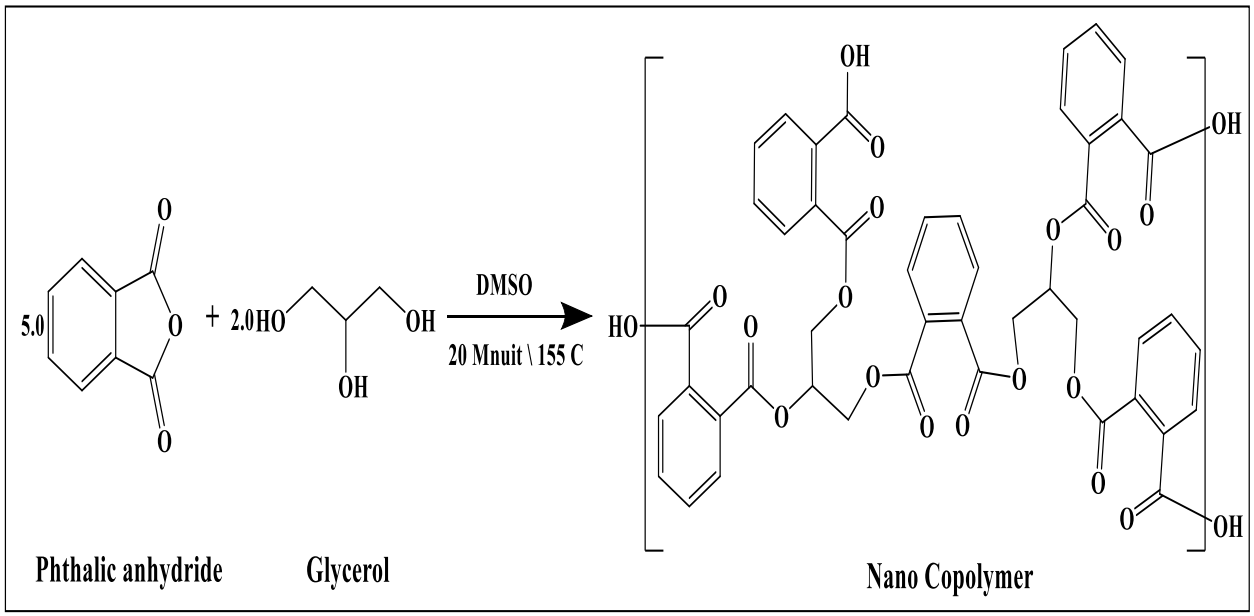

Equation 1: Synthesis of nano copolymer

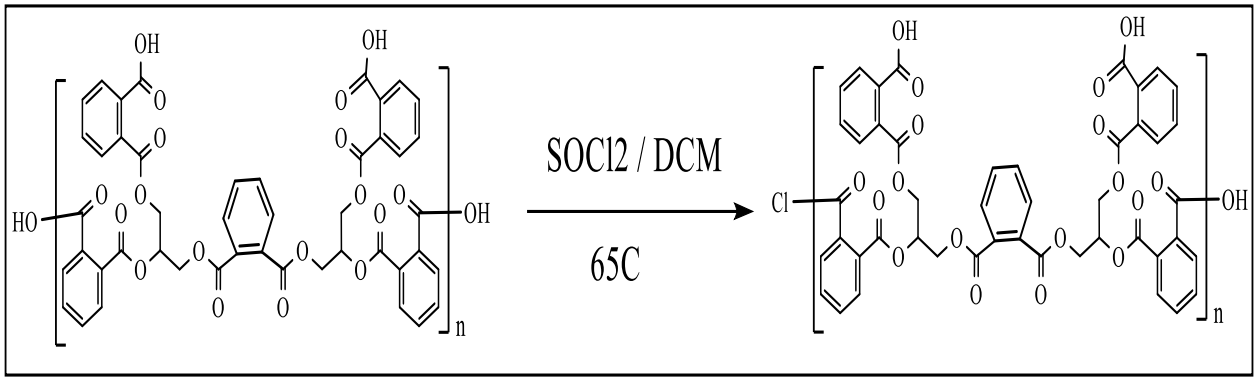

Equation 2: Synthesis of nano copolymer acid chloride

Spectroscopic and Structural Characterization of the Nano Copolymer

FT-IR Analysis (Figure 1):

The FT-IR spectrum of the synthesized nano copolymer confirmed the presence of characteristic functional groups. A broad absorption band between 3550–3200 cm^{-1} corresponds to O–H stretching vibrations of carboxylic acid groups. The aromatic sp^2 C–H stretching vibration appeared at 3057 cm^{-1}, while the aliphatic sp^3 C–H stretching bands were observed at 2998 and 2873 cm^{-1}. A strong band at 1760 cm^{-1} indicates the presence of ester (C=O) linkages, confirming successful esterification. Additionally, a band at 1667 cm^{-1} corresponds to carbonyl stretching vibrations, supporting the formation of the polymer backbone [19,20].

^{1}H NMR Analysis (Figure 2):

The ^{1}H NMR spectrum of the nano copolymer (recorded in DMSO-d_6, 400 MHz) revealed distinct signals corresponding to the polymer structure. A broad singlet at δ = 13.20 ppm was attributed to the hydroxyl protons of the carboxylic acid groups. Multiple peaks between δ = 8.10–7.99 ppm and 7.75–7.68 ppm correspond to aromatic protons from various positions in the polymer framework. A quintet at δ = 2.60–2.59 ppm is assigned to methane group protons, and a doublet at δ = 2.54 ppm corresponds to methylene group protons. These results confirm the expected substitution and aromaticity of the polymer [21,22].

^{13}C NMR Analysis (Figure 3):

The ^{13}C NMR spectrum (DMSO-d_6, 8.15 MHz) further supports the structure of the synthesized nano copolymer. Carbonyl carbon signals were observed at δ = 173.12 ppm and 169.20 ppm, indicating the presence of carboxylic and ester functionalities. Aromatic carbons appeared within the δ = 125–135 ppm range. Signals at δ = 66.8 ppm and 45.23 ppm were assigned to aliphatic carbons, specifically those in methylene and methane environments, verifying the polymer framework and side-chain structures [23,24].

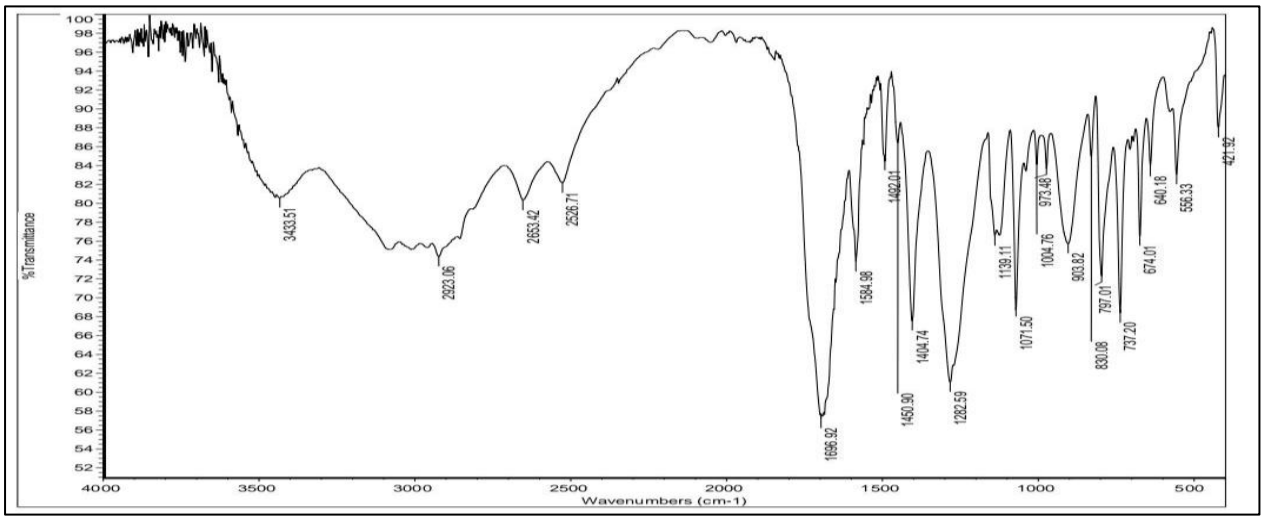

Figure 1: FT-IR spectrum of synthesis nano copolymer

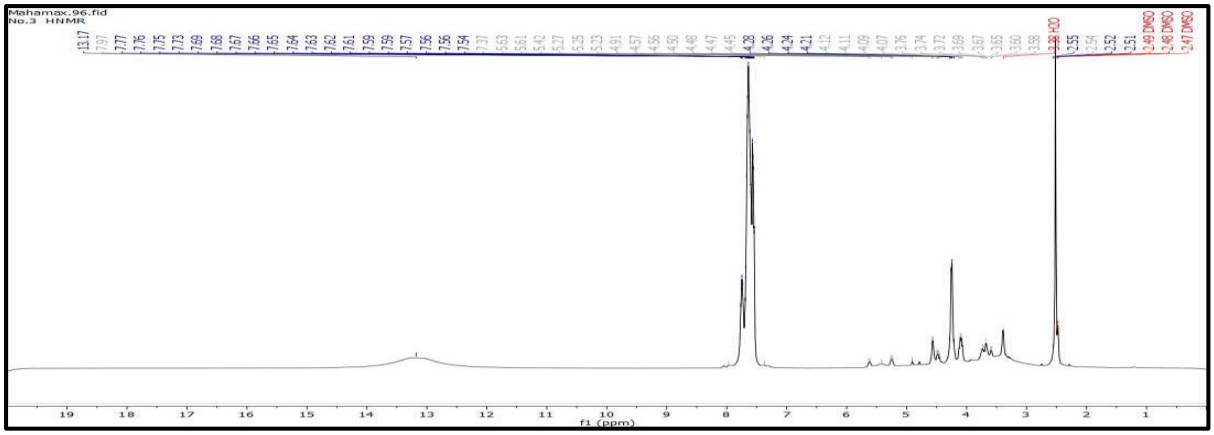

Figure 2: ^{1}H-NMR spectrum of synthesis nano copolymer

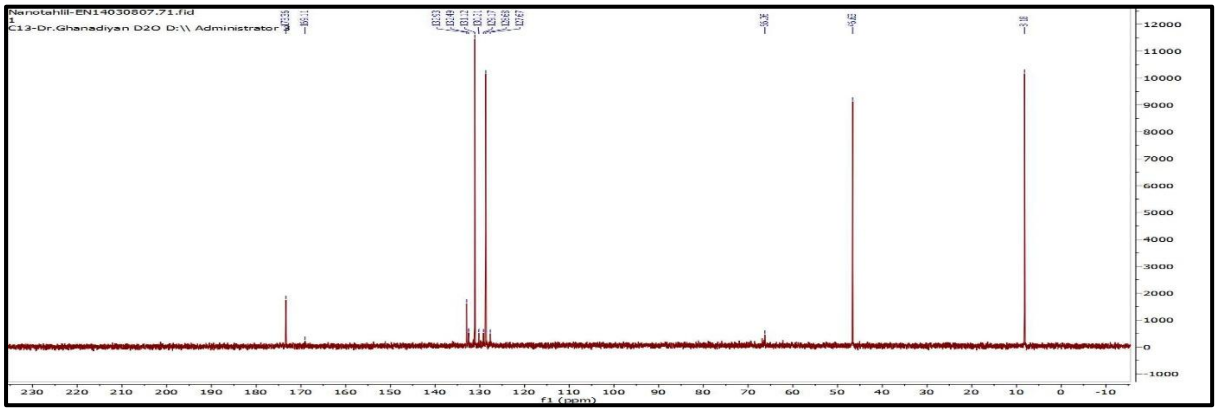

Figure 3: ^{13}CNMR spectrum of synthesis nano copolymer

X-ray Diffraction Analysis (Figure 4):

The XRD pattern of the nano copolymer displayed multiple diffraction peaks at 2θ values of 15.044°, 18.901°, 20.000°, 27.154°, 31.450°, 39.780°, 46.000°, and 47.840°. These peaks indicate a semi-crystalline nature of the material, with moderate crystallinity and minimal amorphous content. The average interplanar spacing (d_{hkl}) was calculated to be 0.569 nm using Bragg's Law:

$$n\lambda=2d\sin(\theta)$$

Where n is the diffraction order, λ is the wavelength of the X-ray source, d is the interplanar spacing, and θ is the diffraction angle [25].

The average crystallite size was determined to be approximately 57.6 nm using the Scherrer equation:

$$D= K\lambda / \beta \cos(\theta)$$

Where D is the crystallite size, K is the shape factor (typically 0.9), λ is the X-ray wavelength, β is the full width at half maximum (FWHM), and θ is the Bragg angle [26]. These results confirm the nanoscale structure and crystalline nature of the synthesized copolymer.

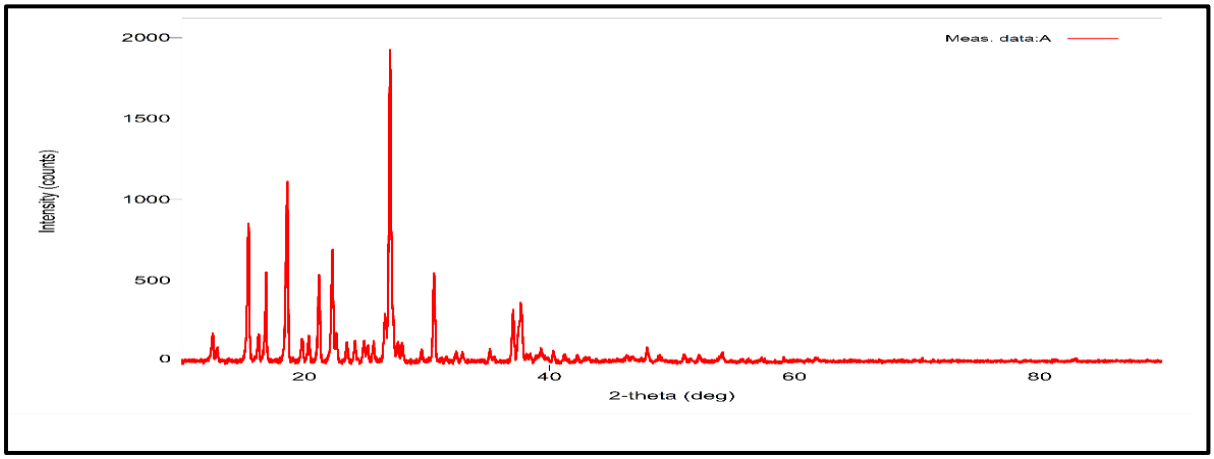

Figure 4: X-Ray spectrograph of nano polymer

International Journal of Environmental Sciences
ISSN: 2229-7359
Vol. 11 No. 22s, 2025
https://theaspd.com/index.php

Table 1: Crystals proportions and the distances of atoms in nano copolymer

2θ	θ	FWHM	D	D	D (EV.)	d(EV.)
15.044	7.5218	0.0778	52.2	0.8140	**57.6**	**0.569**
18.901	9.4505	0.0228	63.0	0.3170		
20.000	10.0000	0.0553	29.9	0.4188		
27.154	13.5770	0.0532	49.0	0.6180		
31.450	15.7250	0.0263	52.6	0.4710		
39.780	19.8900	0.0698	29.3	0.6250		
46.000	23.0000	0.0289	92.4	0.6130		
47.840	23.9200	0.0452	92.4	0.6830		

Surface Morphology and Topography Analysis (AFM)

Figure 5 presents the three-dimensional atomic force microscopy (AFM) images of the synthesized nano copolymer, revealing detailed information about its surface morphology and particle distribution. The surface of the polymer appears uniform with a relatively consistent particle dispersion, supporting the formation of a nanoscale material.

AFM analysis confirmed that the polymer particle sizes fell well within the nanometer range, with measured diameters of approximately **57.04 nm** (Figure 5a) and **23.59 nm** (Figure 5b). This size distribution further validated the successful fabrication of a nanostructured material.

The **roughness coefficient** of the linear nano copolymer surface was calculated to be **29.72 nm**, while the **root mean square (RMS) roughness** value was **60.65 nm**, as illustrated in **Figure 6**. These values confirm the presence of significant surface roughness, a characteristic commonly associated with nanoscale materials. Moreover, the **average particle height** was recorded at **188.9 nm** and **16.52 nm**, further emphasizing the vertical uniformity and nanoscale thickness of the synthesized polymer.

Overall, the AFM analysis supports the conclusion that the synthesized copolymer exhibits nanoscale dimensions, surface homogeneity, and crystalline surface features—key properties that enhance its potential application in drug delivery systems.

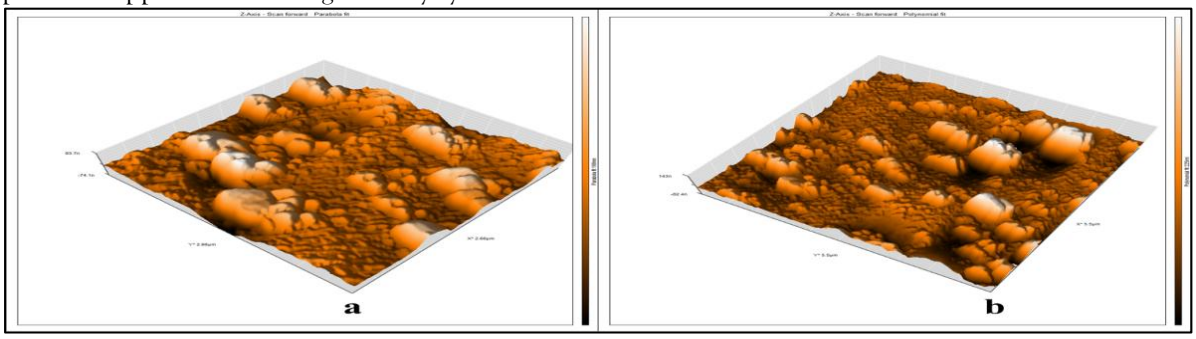

Figure 5: 3D imaging of AFM morphological of nano polymer

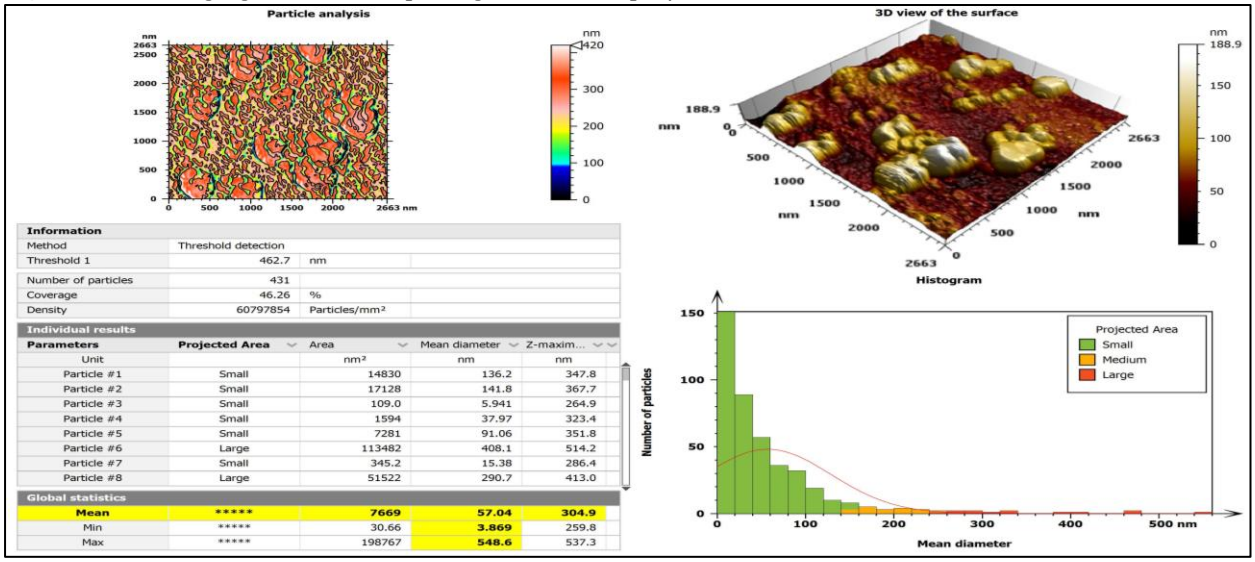

Figure 6: Particle AFM results

Transmission Electron Microscopy (TEM) and Particle Size Distribution

Figure 7 shows the transmission electron microscopy (TEM) images of the synthesized nano copolymer. The images confirm that the copolymer nanoparticles exhibit an average particle size of approximately **57.48 nm**, consistent with the results obtained from XRD and AFM analyses. The nanoparticles were observed in a variety of shapes, including **spherical, discoid, cyclic, crystalline**, and **semi-spherical forms**, indicating structural diversity and possible flexibility in molecular arrangement.

The TEM micrographs captured under both low and high magnification reveal a fairly uniform particle size distribution and smooth surface morphology, further supporting the successful formation of nanoscale particles.

Table 2 presents a detailed quantitative analysis of the particle size, angles, areas, and standard deviations obtained using **ImageJ** software. This data provides statistical validation for the observed dimensions and shape variations.

Figure 8 illustrates the **histogram** representing the frequency distribution of particle sizes. The histogram confirms a relatively narrow size distribution, centered around the mean diameter, supporting the conclusion that the synthesis yielded well-defined and consistently sized nanoparticles suitable for drug delivery applications.

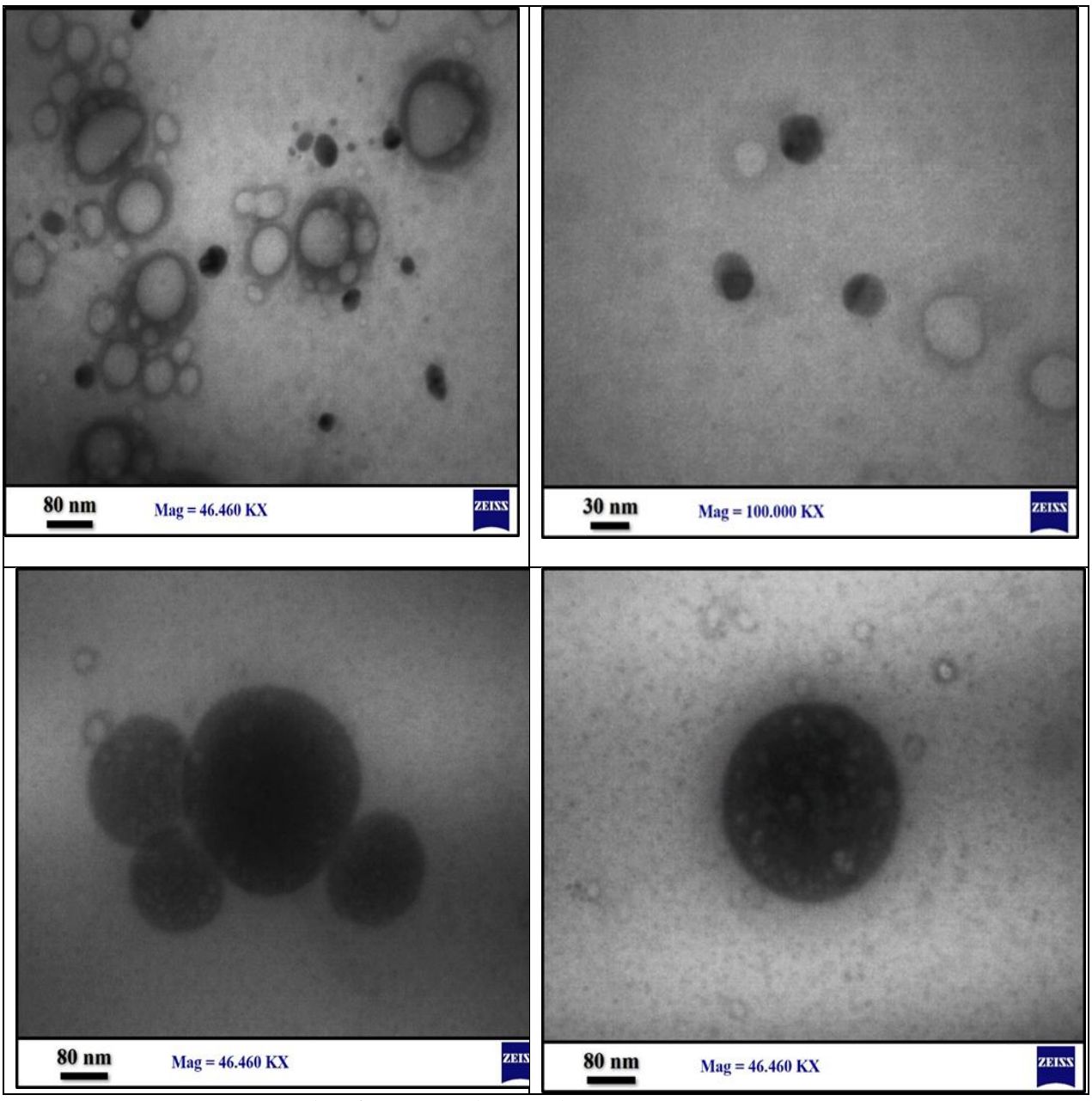

Figure 7: TEM micrographs of nanoparticle's copolymer

Table (2): Proportions diameters, angels and standard deviations of nano polymer

Area	StdDev	Angle	Diameter (nm)	D(av.) nm
13.667	10.551	43.668	40.552	57.48
18.889	8.639	118.989	56.399	
26.111	10.3	91.958	78.046	
15.444	13.99	2.49	46.043	
82	9.659	80.838	80.3	
80	7.232	83.418	78.518	
76	10.278	92.291	75.06	
67	7	95.194	66.272	
43	13.368	94.086	42.107	
80	7.568	26.565	70.01	
46	10.536	24.905	45.019	
3.667	9.511	-34.695	10.541	
93	6.326	-101.31	55.2	
73	17.612	56.976	71.561	
75	3.762	31.759	74.095	
56	7.646	40.601	55.317	
65	11.335	82.405	66.134	

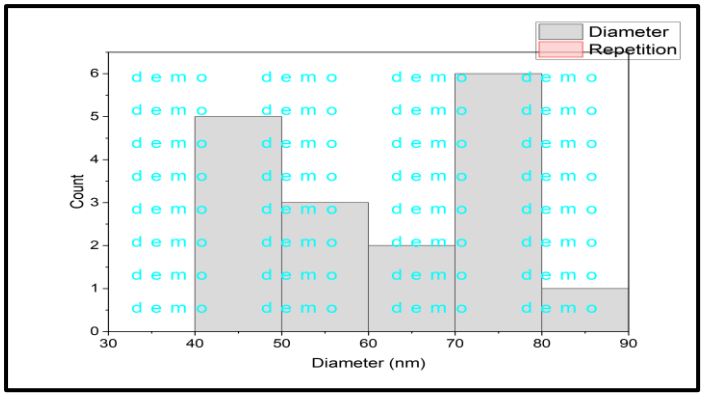

Figure 8: Histogram of different proportions of the particle sizes distribution

Synthesis of a Nano Drug Composite

Reaction was carried out according to the following equation:

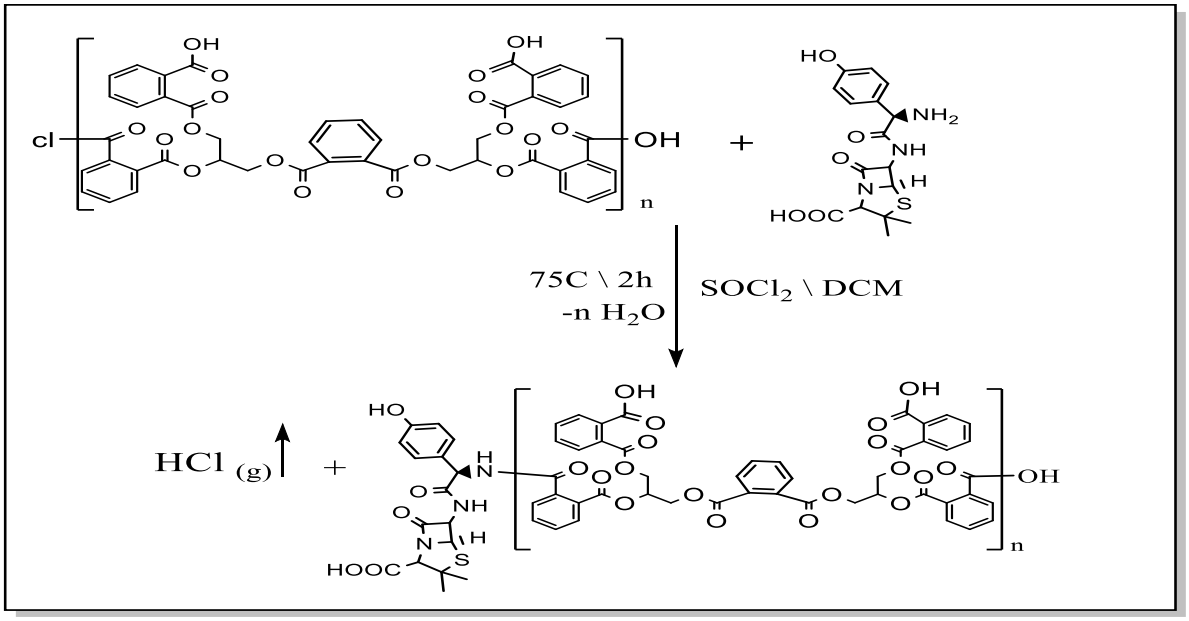

Equation 3: Synthesis of nano drug composite

Yield 75 %, m.p 262 °C, **FT-IR (KBr, cm^{-1}): ν** 2601-3401 carboxylic (OH), 2972 and 2904 (CH, sp^3), 3203 (NH_2), 3017 (CH, sp^2 of aromatic rings), 1516 bend (NH_2), 1458 (bend of CH_2), 1370 (bend of CH_3), 1685 (polymeric ester, C=O), 1667 (carbonyl of secondary amide), 1613 (carbonyl of tertiary amide), Figure 9. **^{1}H NMR (600 MHz, DMSO-d^6) δ** 13.20 (S, COOH), 8.69(s, Ar–OH), 8.22 (s, for the amide group), 7.67-7.53 (m, polymeric aromatic hydrogen's), 7.40-6.27 (m, Drug aromatic hydrogen's), 6.86-6.78 (m, Drug aromatic hydrogen's), 5.90-5.86 (q, Polymeric methane), 5.15-5.12 (d, Hydrogen of atom 69, 93), 4.79-4.77 (d, hydrogen of atom 74, 98), 4.57-4.56 (d, of atom 11, 39, 9 And 31 , 4.36 (hydrogen of atoms 99, 75), 1.74 (s, of Methyl groups). Figure 10. **^{13}C NMR (101 MHz, DMSO-d^6) δ** peak at 176.02 ppm for 72 & 91, 172.50 ppm for carbon 66 &29 , 169.11, ppm for carbon 75 & 99, 166.56 ppm for carbon 56 & 54, 159.53 ppm for carbon 7,13 ,28, 34 ,44 & 18, 155.77 ppm for carbon 26 & 52 , 133.27 ppm for carbon aromatic SP2 , 131.21 ppm for carbon Aromatic sp3 , 130.55 ppm for carbon ph, 130.34 ppm for carbon ph , 128.77 ppm for carbon ph , 115.84 ppm for carbon 62, 60 , 86, & 84 , 115.15 ppm for carbon 85 & 61, 64.84, 72.18 ppm for carbon 75 & 99, 67.48 ppm for carbon 100 & 76, 64.52 ppm for carbon 10 & 31, 57.86 ppm for carbon 98 & 76, 53.16 for carbon 63 & 69, 49.94 ppm for carbon 88 & 66, 25.58 ppm for 79, 80, 104 & 103. Figure 11.

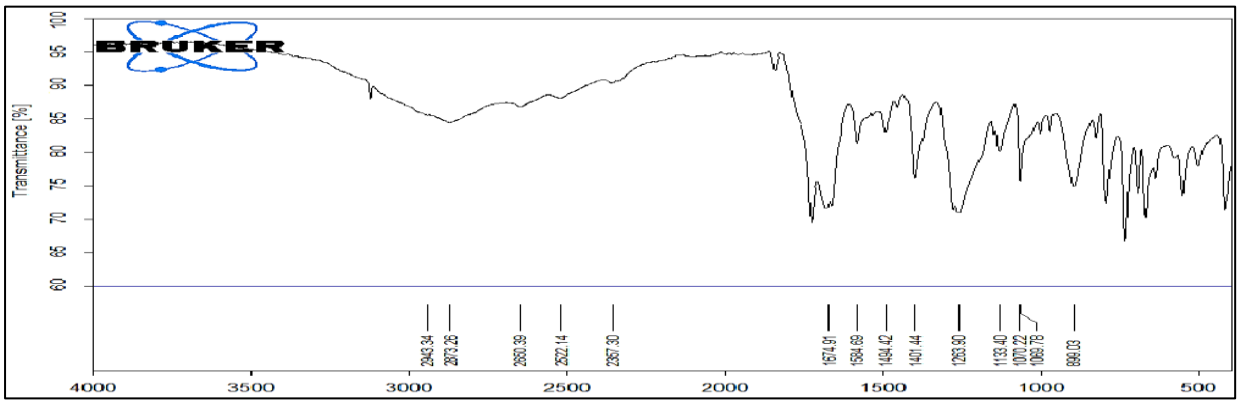

Figure 9: FT-IR spectrum of nano drug composite

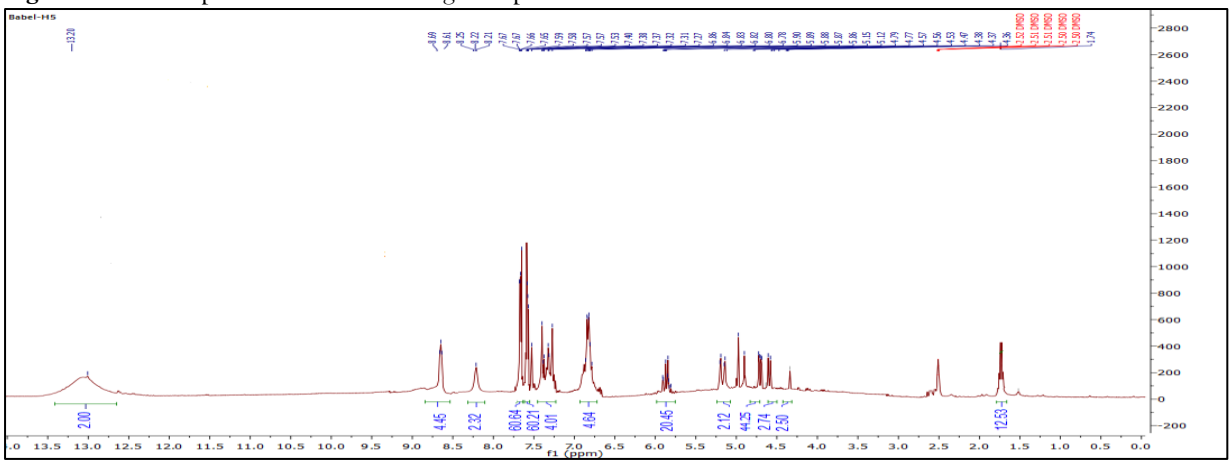

Figure 10: ^{1}H-NMR spectrum of nano drug composite

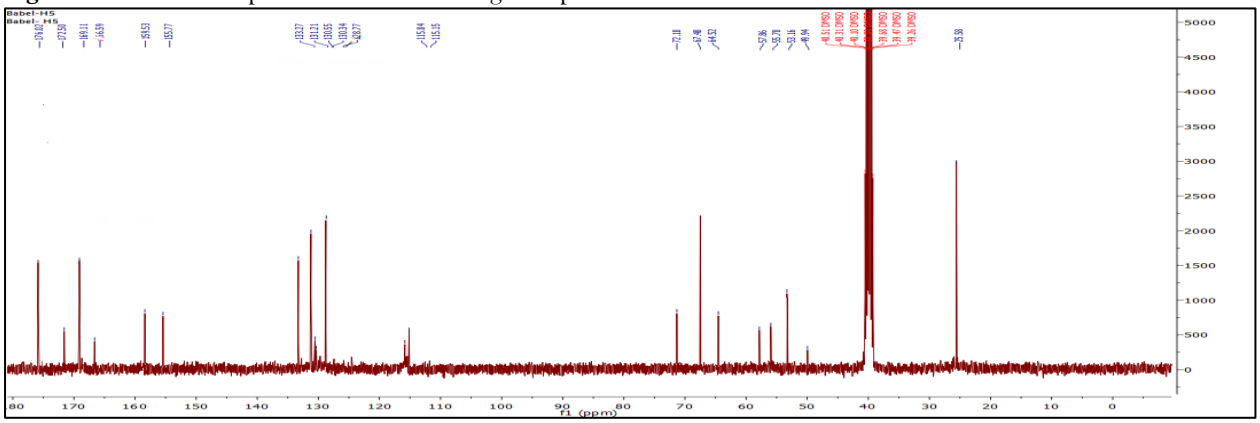

Figure 11: ^{13}C-NMR spectrum of nano drug composite

International Journal of Environmental Sciences
ISSN: 2229-7359
Vol. 11 No. 22s, 2025
https://theaspd.com/index.php

Molecular Docking of the Drug Composite

Table 4 summarizes the molecular docking results of the synthesized nano drug composite (H5) with the target protein chain (PDB ID: **1JNX**), including calculated binding energies and root mean square deviation (RMSD) values. These parameters provide insights into the binding affinity and stability of the drug–protein complex.

Figure 12 illustrates the docking interaction between the nano drug composite and the amino acid residues of the 1JNX protein. Notably, **aspartic acid (Asp, X:1813)** and **glutamic acid (Glu, X:1836)** formed ***π*-alkyl interactions** with the drug, indicated in light purple. These hydrophobic interactions contribute significantly to the binding stability.

A **repulsive interaction** (visualized in red) was observed between the electron-rich regions of the drug molecule and **tyrosine (Tyr, X:1653)**, suggesting a potential steric or electronic hindrance at this site.

Several **hydrogen bonds** (colored dark green) were identified between the drug and key polar amino acid residues including **leucine (Gly, X:1854)**, **glutamine (Gln, X:1848)**, **aspartic acid (Asp, X:1840)**, and **threonine (Ser, X:1852)**. These interactions play a crucial role in the specificity and strength of the ligand–receptor binding.

Additionally, **C–H bonds** (light green) were observed with **proline (X:856)** and **valine (Ser, X:1741)**. The remaining amino acids—**phenylalanine (Phe), arginine (Arg), asparagine (Asn), methionine (Met), leucine (Leu),** and **glutamine (Gln)**—contributed to **van der Waals interactions**, providing further stabilization to the complex.

Figure 13 presents the types and lengths of all molecular bonds formed between amoxicillin and the amino acids of the 1JNX protein. **Figure 14** highlights the specific regions where **hydrogen bonding** occurs, indicating critical areas of drug–target interaction.

These findings suggest that the nano drug composite forms multiple strong and specific interactions with the breast cancer-related protein, supporting its potential effectiveness as a therapeutic agent.

Table 4. Binding energy of drug composite (H5) with amino acids

Ligand	inding Affinity (kcal/mo	Mode	MSD lower boun	RMSD upper bound
7zav_a4.cdx_uff_E=3317.62	-5.9	0	0.0	0.0
7zav_a4.cdx_uff_E=3317.62	-5.6	1	24.939	29.542
7zav_a4.cdx_uff_E=3317.62	-5.5	2	53.285	58.375
7zav_a4.cdx_uff_E=3317.62	-5.4	3	4.331	9.694
7zav_a4.cdx_uff_E=3317.62	-5.4	4	49.677	54.678
7zav_a4.cdx_uff_E=3317.62	-5.2	5	3.445	9.362
7zav_a4.cdx_uff_E=3317.62	-5.2	6	52.785	58.075
7zav_a4.cdx_uff_E=3317.62	-5.2	7	25.974	31.51
7zav_a4.cdx_uff_E=3317.62	-5.2	8	4.881	9.83

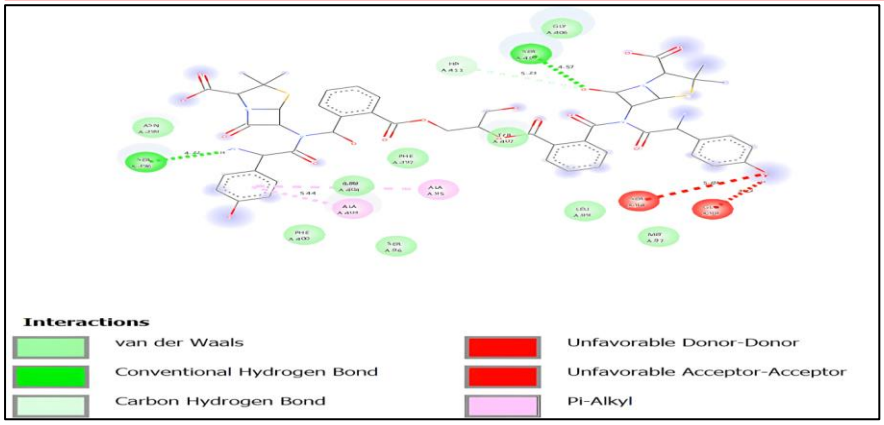

Figure 12: Bonds formed between the protein of cancer cells and the drug composite

International Journal of Environmental Sciences
ISSN: 2229-7359
Vol. 11 No. 22s, 2025
https://theaspd.com/index.php

Also given according to the donor part and the acquired part according to the figures below (13). The drug amoxicillin appears to be polymer-linked to the amino acids found in the breast cancer protein. Cohesion is given according to the basic part and the acidic part also according to the figure below (14). The cohesion of the drug amoxicillin bound to the polymer appears with the amino acids found in the breast cancer protein according to the acidic and basic groups.

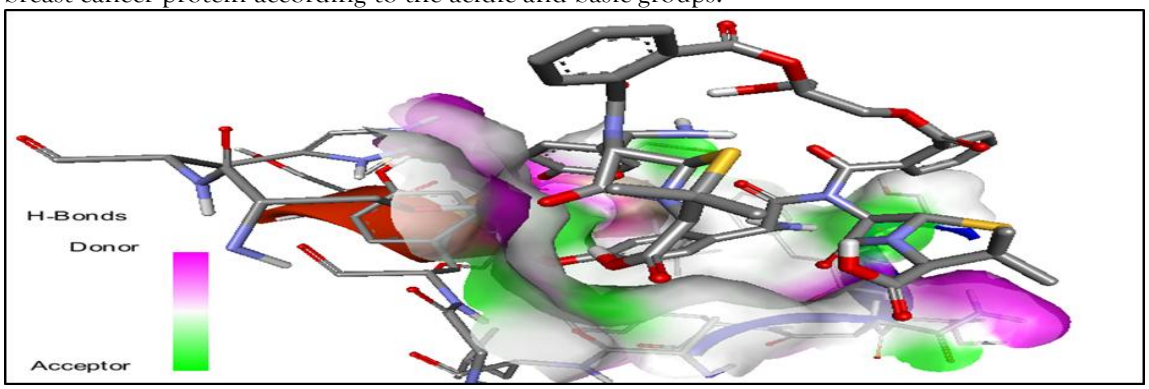

Figure 13: Binding of the drug (H5) bound to the protein of cancer cells.

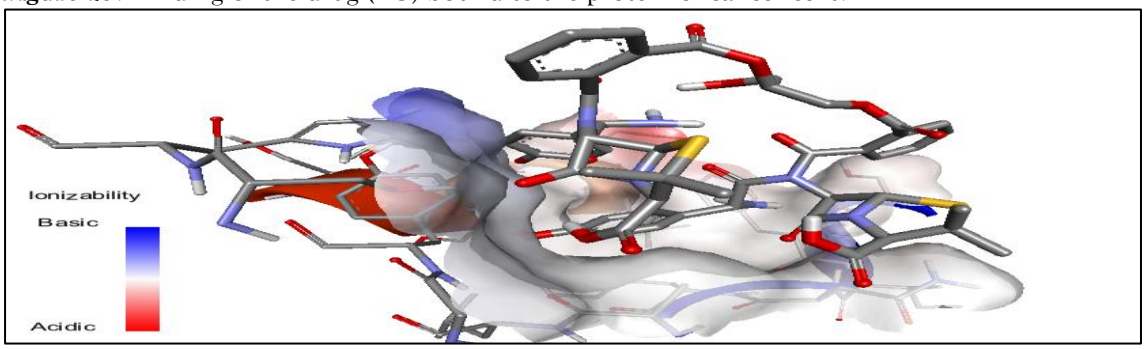

Figure 14: Binding of the drug composite (H5) bound to the protein of cancer cells.

The potential of nano-chitosan as an inhibitor of cancer cells, particularly liver cancer cell lines, is closely linked to its hydrogen bonding capacity [16]. Hydrogen bonding enhances its biological activity by promoting stronger interactions with target enzymes, improving cell permeability, inducing cancer cell death, and increasing selectivity toward cancer cells. Therefore, developing derivatives with optimized hydrogen bonding properties could lead to more effective and safer anticancer therapies [27, 28].

Anti-Cancer Measurements

The anti-cancer potential of the prepared formulation was assessed against MCF-7 breast cancer cells. As shown in Figure 15, untreated cells (Figure 15a) exhibited normal morphology, high density, and intact membranes. In contrast, cells treated with the drug-loaded copolymer H5 (Figure 15b) showed pronounced morphological alterations, including reduced cell density, membrane disruption, and structural damage.

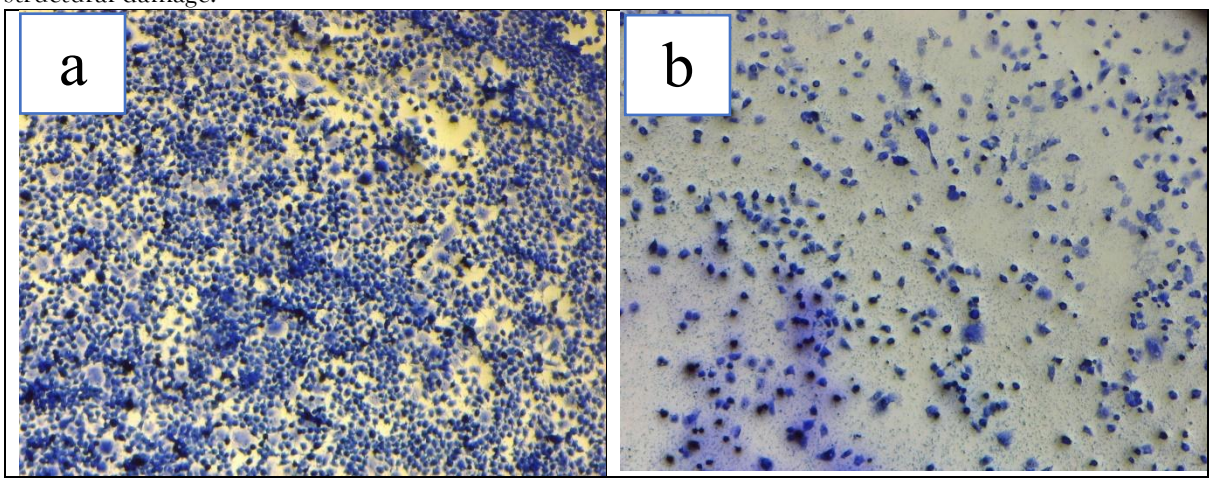

Figure (15): Picture represent; untreated cancer cells (a), treated cancer cells (b)

The cytotoxicity profile of H5 (Figure 16) revealed a clear dose-dependent inhibition of MCF-7 cell proliferation, with an IC_{50} value of 55.09 µg/mL, demonstrating strong anti-proliferative activity. These findings are consistent with previous reports [29], where untreated cells appeared densely packed with irregular shapes and no swelling.

Post-treatment morphology in this study also mirrors earlier observations [30], showing a substantial decrease in cell number, distorted and swollen cells, and the appearance of dark spots indicative of debris from lysed cells. Such morphological changes strongly support the cytotoxic and cell-destructive effects of H5 on MCF-7 breast cancer cells.

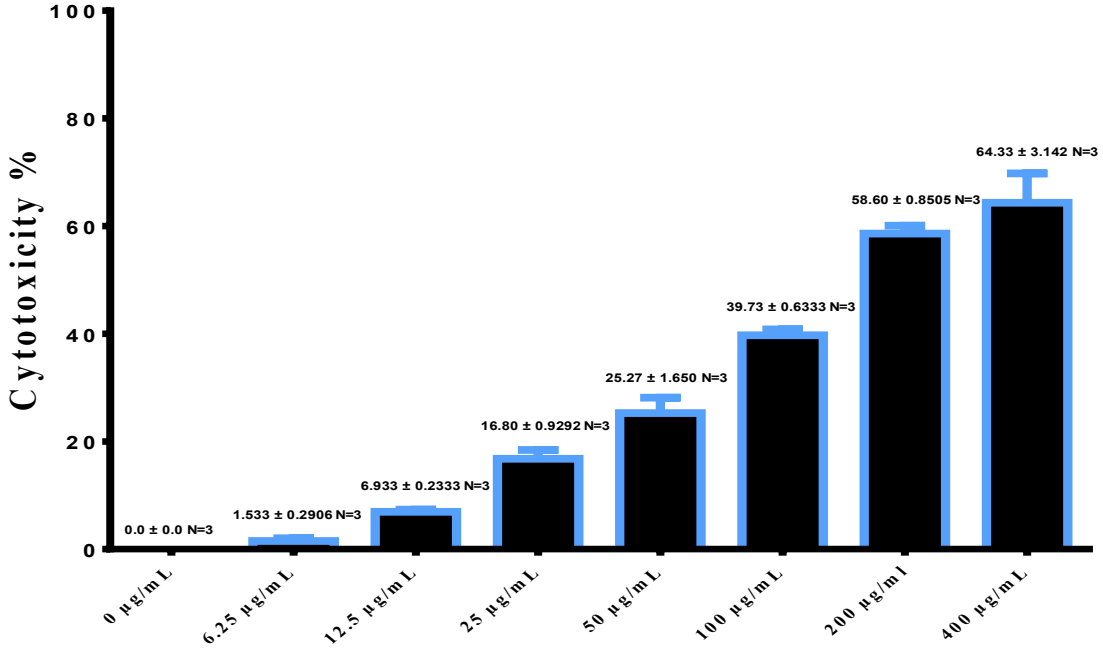

Figure 17: Cytotoxicity effect of H5 in MCF-7 cells. Data are represented as mean ± SD. IC50=55.09 µg/ml

CONCLUSION

Comprehensive physicochemical characterization through FT-IR, NMR, XRD, TEM, and AFM confirmed the successful synthesis and nanostructuring of the polymer. The material exhibited an average crystal size of 57.6 nm, a d-spacing of 0.569 nm, and a surface roughness of 29.72 nm, all indicative of a well-defined nano-architecture. These nanoscale features are directly linked to its efficiency as a drug delivery carrier, enhancing the physicochemical stability, solubility, and biological performance of amoxicillin.

Hydrogen bonding interactions with target biomolecules in cancer cells were identified as a critical factor in its anticancer efficacy. The engineered nano-carrier provided precise breast cancer cell targeting, increasing therapeutic selectivity and minimizing undesirable off-target effects. Such targeted delivery mechanisms are particularly valuable in oncology, where collateral damage to healthy cells often limits treatment effectiveness.

Biological evaluation through in vitro assays against the MCF-7 breast cancer cell line demonstrated potent anti-proliferative activity, with an IC_{50} value of 55.09 µg/mL. Microscopic analyses revealed distinct morphological alterations, including cell shrinkage, membrane damage, and the formation of dark spots corresponding to lysed cellular debris, further validating its cytotoxic potential.

Beyond anticancer performance, the nano-engineered carrier offered significant pharmaceutical advantages. It improved drug stability, enhanced bioavailability, and protected amoxicillin from enzymatic degradation, thereby prolonging its therapeutic activity. These improvements collectively address key challenges in drug delivery systems, such as rapid drug clearance, low solubility, and systemic toxicity.

The present findings not only establish the promise of nano-engineered antibiotics in breast cancer therapy but also open new avenues for the repurposing of existing drugs through nanotechnology-based modifications. Future studies should focus on in vivo evaluations, long-term toxicity assessments, and potential combination therapies to fully realize the clinical potential of such systems. By bridging

pharmaceutical nanotechnology with oncology, this approach represents a step forward in developing safer, more effective, and targeted cancer treatments.

Future Outlook

Building on these promising in vitro results, future research should prioritize comprehensive in vivo studies to evaluate the safety, pharmacokinetics, and therapeutic efficacy of the nano-engineered amoxicillin formulation. Long-term toxicity assessments will be critical to ensure biocompatibility and minimize adverse effects. Moreover, exploring combination therapies with other anticancer agents could enhance treatment outcomes through synergistic mechanisms.

Advancements in nanotechnology offer exciting opportunities to repurpose existing antibiotics, expanding their applications beyond infectious diseases to targeted cancer therapies. Continued optimization of nanocarrier design, including surface functionalization for improved targeting and controlled drug release, will further enhance clinical potential.

Ultimately, integrating such nano-engineered drug delivery systems into standard oncology protocols may significantly improve patient outcomes by providing safer, more selective, and effective cancer treatments. This study lays a strong foundation for the development of next-generation nanomedicines that harness the versatility of antibiotics for innovative cancer therapy.

Data availability

All data have been given in the article and Supplementary Information.

REFERENCES:

[1] K. I. Ab, A. H. Abbas, A. S. Abed, and M. N. Bahjat AL-Baiati, "Nano-Poly Chitosan-Ampicillin Drug: Synthesis, Characterization and Cytotoxicity," Egyptian Journal of Chemistry, vol. 65, no. 131, pp. 1313-1318, 2022, doi: https://doi.org/https://dx.doi.org/10.21608/ejchem.2022.150425.6518

[2] O. Abdulnabi, H. Alsalame, and M. Al-baiati, "Studying of Using Chitosan-Cephalexin Nano composed to Induce ROS and Apoptosis in Colon Cancer Cell Line HCT-29," Moroccan Journal of Chemistry, vol. 12, no. 3, pp. 1270-1280, 2024, doi: https://doi.org/https://doi.org/10.48317/IMIST.PRSM/morjchem-v12i3.48702.

[3] A. A. Abdulridha, N. A. Abdul-Rida, and M. N. AL-Baiati, "Synthesis of novel nano co-polymer as pH sensitive drug delivery system, experimental and theoretical study," in AIP Conference Proceedings, 2023, vol. 2414, no. 1: AIP Publishing.

[4] A. A. Abdulridha, N. A. Abdul-Rida, and M. N. AL-Baiati, "Controlled drug delivery and release by new nanopolymer, experimental and theoretical study," in AIP Conference Proceedings, 2023, vol. 2414, no. 1: AIP Publishing, doi: https://doi.org/10.1063/5.0114490.

[5] Z. M. A. Al-Aama, H. Q. AL-Masoudi, A. A. Abdulridha, K. I. Abd Nusaif, and M. N. AL-Baiati, "Synthesis of a smart nano graft co-polymer as a drug delivery," in AIP Conference Proceedings, 2023, vol. 2414, no. 1: AIP Publishing, doi: https://doi.org/10.1063/5.0114726.

[6] A. R. Khudhair, S. T. H. Sherazi, and M. N. Al-Baiati, "Adsorption of methylene blue from aqueous solutions by using a novel nano co-polymer," in AIP Conference Proceedings, 2020, vol. 2290, no. 1: AIP Publishing, doi: https://doi.org/10.1063/5.0027741.

[7] A. H. Athab, A. H. Al-Safy, and M. N. Al-Baiati, "Study of the Effective Range of Drug Level Using a Novel Nano Co-polymer-Mefenamic Acid," International Journal of Drug Delivery Technology, vol. 12, no. 04, pp. 1808-1813, 2022, doi: https://doi.org/10.25258/ijddt.12.4.53.

[8] K. I. Abd and H. A. Ali, "Identifying the LBP and insulin resistance: potential role for the increased feto-maternal morbidity and long-term complications," Biochemical & Cellular Archives, vol. 20, no. 2, 2020.

[9] K. M. H. Khawla I. Abd N., Sara A. M., Inam J. R., , "Association between sex hormonal and metabolic changes in female with infertility, in Al-Najaf city patients, ," Ginekologia i Poloznictwo, , vol. 4, no. 68, pp. 001-005, 2024.

[10]B. Al-Ghanimi, K. Abd Nusaif, and M. Al-Baiati, "Novel nano chitosan loaded with amoxicillin as inhibitor lung cancer cell line (A549): Biological activity and molecular studies, Moroccan J," J. Chem, vol. 13, no. 2, pp. 480-494, 2025, doi: https://doi.org/10.48317/IMIST.PRSM/morjchem-v13i2.49619.

[11]Z. M. Shakir, M. M. Kareem, and M. N. Al-Baiati, "Inhibition of spread of the breast cancer by using of some nano co-polymer-drugs," in AIP Conference Proceedings, 2023, vol. 2414, no. 1: AIP Publishing, doi: https://doi.org/10.1063/5.0114719.

[12]M. F. Anad, H. E. Salman, and M. N. Al-Baiati, "Synthesis a novel nano graft co-polymer and studying the swelling behaviors using different molar ratios of acrylic acid monomer," in IOP Conference Series: Materials Science and Engineering, 2019, vol. 571, no. 1: IOP Publishing, p. 012096, doi: https://doi.org/10.1088/1757-899X/571/1/012096.

[13]M. N. AL-Baiati, N. N. Jafar, and R. H. Zaooly, "Study The Effect Verifies of the Number of Moles of Acrylic Acid Monomer On Swelling of the New Prepared Modified Co-Polymer," RESEARCH JOURNAL OF PHARMACEUTICAL BIOLOGICAL AND CHEMICAL SCIENCES, vol. 7, no. 5, pp. 1452-1463, 2016.

[14]O. Abdulnabi, H. Alsalame, and M. Al-baiati, "Preparation and Characterization a Nano Chitosan-Mefenamic acid Composites as Biocompatible Treatment Anti-Colon Cancer Cell line HCT-29," Moroccan Journal of Chemistry, vol. 13, no. 1, pp. 366-380, 2025, doi: https://doi.org/10.48317/IMIST.PRSM/morjchem-v13i1.49451.

[15]M. M. Obaid and M. N. Al-Baiati, "Studying the effectiveness of using a novel nano polymer as a protein delivery system," in AIP Conference Proceedings, 2023, vol. 2414, no. 1: AIP Publishing, doi: https://doi.org/10.1063/5.0114723.

[16]B. K. Al-Ghanimi, K. I. Abd, M. N. Al-Baiati, H. H. Al-Ghanimi, and R. A.-A. Al-Madany, "Using a Novel Nano Chitosan Ampicillin Drug as a Treatment for Lung Cancer Cell Line (A549)," Arabian Journal of Medicinal and Aromatic Plants, vol. 10, no. 2, pp. 1-21, 2024.
[17]S. F. Hassan, Z. T. Habeeb, and M. N. AL-Baiati, "Synthesis and Characterization a Novel Nano Co-polymer-Drugs Composites and using it as Treatment to Liver Cancer," Moroccan Journal of Chemistry, vol. 13, no. 1, pp. 106-121, 2025, doi: https://doi.org/10.48317/IMIST.PRSM/morjchem-v13i1.50079.
[18]Z. M. Shakir, M. M. Kareem, and M. N. Al-Baiati, "Study the effects of some nano graft co-polymer-drugs on the spread of breast cancer," in AIP Conference Proceedings, 2023, vol. 2414, no. 1: AIP Publishing, doi: https://doi.org/10.1063/5.0114710.
[19]Q. Xu, H. Pan, W. Zhang, L. Xu, and T. Li, "Preparation and photocatalytic performance of TiO2/lignin-based carbon composited photocatalyst," in Journal of Physics: Conference Series, 2024, vol. 2671, no. 1: IOP Publishing, p. 012013.
[20]A. Huang, Q. Zhou, J. Liu, B. Fei, and S. Sun, "Distinction of three wood species by Fourier transform infrared spectroscopy and two-dimensional correlation IR spectroscopy," Journal of Molecular Structure, vol. 883, pp. 160-166, 2008.
[21]L. Wiese, "Total Synthesis of the Antiviral Natural Products Cleistocaltone A and B," 2024.
[22]A. F. Frank, "The Design, Synthesis, and Characterization of Gallium-Salophen Complexes (GaSal-3) as Inhibitors of Pseudomonas aeruginosa Heme Sensing and Utilization System," University of Maryland, Baltimore, 2025.
[23]C. Y. Ma, Y. Xu, L. H. Xu, C. Zhang, J. Y. Qi, and J. L. Wen, "NMR Characterization of Lignin," Lignin Chemistry: Characterization, Isolation, and Valorization, pp. 15-60, 2024.
[24]D. S. Khachatryan et al., "Novel derivatives of thiohydantoin-containing tetrahydro-β-carboline possess activity against influenza virus at late stages of viral cycle without affecting viral neuraminidase," Archiv der Pharmazie, vol. 358, no. 3, p. e2400733, 2025.
[25]M. R. Caruso, G. Cavallaro, S. Milioto, and G. Lazzara, "Halloysite nanotubes/Keratin composites for wool treatment," Applied Clay Science, vol. 238, p. 106930, 2023.
[26]A. Monshi, M. R. Foroughi, and M. R. Monshi, "Modified Scherrer equation to estimate more accurately nano-crystallite size using XRD," World journal of nano science and engineering, vol. 2, no. 3, pp. 154-160, 2012.
[27]Z. T. Habeeb, K. I. Ab, and M. S. Naser, "Monitoring Study on the Incidence of 25-OH Vitamin D Deficiency in Population of Kerbala Province," Egyptian Journal of Chemistry, vol. 65, no. 131, pp. 1319-1322, 2022, doi: https://doi.org/10.21608/EJCHEM.2022.150424.6517.
[28]A. Khaldan et al., "Aspirin-Loaded Chitosan Nanoparticles: A Breakthrough in Liver Cancer Therapy," Heliyon, vol. 7, no. 3, 2021, doi: https://doi.org/10.1016/j.heliyon.2021.e06603.
[29]Y. Hao et al., "Exopolysaccharide from Cryptococcus heimaeyensis S20 induces autophagic cell death in non-small cell lung cancer cells via ROS/p38 and ROS/ERK signalling," Cell proliferation, vol. 53, no. 8, p. e12869, 2020.
[30]Y. Jin et al., "Hydroponic Ginseng ROOT Mediated with CMC Polymer-Coated Zinc Oxide Nanoparticles for Cellular Apoptosis via Downregulation of BCL-2 Gene Expression in A549 Lung Cancer Cell Line," Molecules, vol. 28, no. 2, p. 906, 2023.